Fluctuation De-trending and Autocorrelation:

The fluorescence of an individual cell tracked over time is composed of two components: (1) a stochastic signal related to the structure and parameters of the underlying gene circuit; and (2) a component related to basal gene expression and response to external stimuli (e.g. chemical induction using Tat or TNF-α; see Supplementary Fig. 1 below). Autocorrelations functions are calculated using only this stochastic component, which we call $\tilde{N}_m(t)$, that must first be extracted from the measured total fluorescence intensity. This extraction requires a 3-step process consisting of each of the following: (1) removal of signal components related to external stimuli; (2) normalizing the fluctuations to the mean level of gene expression; and (3) removing the baseline of each signal so that it is zero mean over the duration of the experiment. Step (1) is required to prevent corruption of the noise autocorrelation by the external stimulus signal; step (2) ensures that a fluctuation of 1 a.u. of fluorescence from a baseline of 10 a.u. of fluorescence carries the same weight as a fluctuation of 10 a.u. of fluorescence from a baseline of 100 a.u. of fluorescence; and step (3) is required to prevent the calculation of erroneously long autocorrelations due to inaccuracies in the baseline of signals from individual cells because of differences in basal gene expression levels. Step (3) is described in more detail in the next section.

Mathematically this procedure may be stated as follows:

$$N_m(kT_s) \equiv \left(I_m(kT_s) - g_m \cdot A(kT_s)\right) / S_m(kT_s)$$

$$\tilde{N}_m(kT_s) \equiv N_m(kT_s) - \frac{1}{K+1}\sum_{k=0}^{K} N_m(kT_s)$$

where:

T_s is the time interval between measurements of fluorescent intensity and $k = 0, 1, 2, ... K$ is the sample number.

$m = 1, \ldots, M$, represents each of the M single cells sampled in an experiment.

$I_m(t)$ is the time-dependent fluorescent intensity measured for each cell $m = 1, \ldots, M$.

$A(kT_s) = \frac{\sum_{m=1}^{M} I_m(kT_s)}{M}$, is the time dependent average fluorescence from all of the tracked cells. We refer to $A(t)$ as the general trend and it is meant to capture changes in gene expression levels over time that affect all of the cells but are not related to the stochastic behavior of the underlying gene circuits.

g_m is a gain factor that describes the extent to which the general trend couples into each individual noise trajectory. As many of our experiments began with the addition of a chemical inducer, we assumed that all cells behaved according to the general trend $A(kT_s)$, but were scaled differently (perhaps due to different sizes, different focal planes or small variations in local conditions across the cell culture). The g_m values were selected to minimize the cross-correlation between $N_m(kT_s)$ and $A(kT_s)$, or more explicitly the g_m which minimized $\left| \sum_{k=0}^{k=K} N_m(kT_s) \cdot \tilde{A}(kT_s) \right|$, where $\tilde{A}(kT_s) = A(kT_s) - \overline{A(kT_s)}$ and $\overline{A(kT_s)}$ was the average value of $A(kT_s)$ over the duration of the experiment. $\tilde{A}(kT_s)$ is

used instead of $A(kT_s)$ in this calculation to avoid errors in the g_m calculation due to correlations between the baselines (average values) of $N_m(kT_s)$ and $A(kT_s)$.

$S_m(kT_s)$ is used for the normalization of fluctuations when the gene expression level changes significantly during the experiment (e.g. large changes in expression due to the addition of an inducer). If the gene expression level changed very little during the experiment (e.g. no inducer added), $S_m(kT_s)$ was simply set to a constant. For larger excursions a reasonable approach would be to set $S_m(kT_s) = g_m A(kT_s)$; however this approach may lead to errors due to division by small values as a few trajectories have small g_m values. To prevent these errors we considered two approaches: (1) trajectories with gm << 1 could be discarded or (2) $S_m(kT_s)$ could be set equal to $A(kT_s)$ for all trajectories. The first approach gives trajectories with low g_m no weight in determining the composite autocorrelation function, while the second approach gives them a reduced weight. Although we saw little difference in the $\tau_{1/2}$ values obtained using the two approaches, we used the second approach as it allowed the inclusion of a few more noise trajectories.

Each of the three processing steps is illustrated in Supplementary Figure 1.

The normalized composite autocorrelations were processed for all experiments using a biased algorithm[8] similar to that previously described in [9]:

$$\Phi_m(jT_s) = \frac{\sum_{k=0}^{K-j} \tilde{N}_m(kT_s)\tilde{N}_m((k+j)T_s)}{\sum_{k=0}^{K} \tilde{N}_m^2(kT_s)},$$

where j had integer values from 0 to K-1. The composite autocorrelation function (Φ_c) for M cell trajectories was found using

$$\Phi_c(jT_s) = \frac{\sum_{m=1}^{M}\sum_{k=0}^{K-j}\tilde{N}_m(kT_s)\tilde{N}_m((k+j)T_s)}{\sum_{m=1}^{M}\sum_{k=0}^{K}\tilde{N}_m^2(kT_s)}$$

The total number of cells collected from segmentation of the time-lapse microscopy image stacks were between 30-100 cells depending on the experiment. Importantly, an ensemble of 30 cells was found sufficient for estimating the high frequency half-correlation time (see discussion on error bar estimation below).

One concern was that the additional processing (i.e. removal of the transient and scaling) for experiments where exogenous Tat or TNF-α were used could produce correlation artifacts that would reduce the accuracy of our calculated ACFs. The three different experimental conditions (no drug, +Tat, and + TNFα) did produce $\tau_{1/2}$ values that did differ by slightly more than the error bars (1.2 hours, 1.37 hours, and 1.29 hours, respectively for the no feedback cases; 1.59 hours, 1.77 hours, 1.67 hours for the positive feedback cases). These small variations may be due to processing artifacts or to different induction mechanisms that have moderately different basal noise characteristics. However, these differences are small enough that they may safely be neglected in this study. Furthermore, the important parameters are the feedback-mediated shifts in the $\tau_{1/2}$ values as compared to their respective no feedback controls, and these shifts were quite uniform for the no drug, +Tat, and + TNF-α cases (see summary table at the end of this document). Likewise for the +Tat, and + TNF-α experiments, scaling by $A(kT_s)$ instead of $g_m A(kT_s)$ had a relatively modest effect on the $\tau_{1/2}$ values as shown in the table below. The $\tau_{1/2}$ shifts were in the same direction and of similar magnitudes for both scaling methods;

however for $g_m\,A(kT_s)$ scaling, $\tau_{1/2}$ values were strongly biased by a few trajectories with small g_m values.

Scale factor	$\tau_{1/2}$ (hours; +FB/NFB), + TNF-α	$\tau_{1/2}$ (hours; +FB/NFB), +Tat
$A(kT_s)$	1.67/1.29	1.77/1.37
$g_m\,A(kT_s)$	1.85/1.29	2.03/1.01

Baseline Suppression and High Frequency Autocorrelation Functions

As described above, the $N_m(kT_s)$ terms still required a correction to remove deterministic components not related to the general trend. These signal components are most likely related to differences in basal gene expression levels, which may vary widely due to different chromosomal integration sites and variations in local environments for the cells. In general we may write that (note: for convenience we do this analysis for continuous time (not sampled) signals, but the conclusions apply to the autocorrelation functions calculated as described above)

$$\tilde{N}_m(t) = N_m(t) - D_m(t),$$

where in the ideal case $\tilde{N}_m(t)$ is a zero-mean random process representing the stochastic fluctuations in gene expression. If $D_m(t)$ is a true representation of only the deterministic portion of $N_m(t)$

$$\lim_{T_W\to\infty}\frac{1}{T_W}\int_0^{T_W}\tilde{N}_m(t)dt = \lim_{T_W\to\infty}\frac{1}{T_W}\int_0^{T_W}\left(N_m(t) - D_m(t)\right)dt = 0,$$

which implicitly defines $D_m(t)$ through the expression

$$\lim_{T_W \to \infty} \frac{1}{T_W} \int_0^{T_W} D_m(t)dt = \lim_{T_W \to \infty} \frac{1}{T_W} \int_0^{T_W} N_m(t)dt \,.$$

However, this definition is of little utility as cell trajectories may only be traced over limited time periods, $\tilde{T}_W$, and in general even for the ideal case

$$\frac{1}{\tilde{T}_W} \int_0^{\tilde{T}_W} \tilde{N}_m(t)dt \neq 0 \,.$$

unless $\tilde{T}_W$ >> dominant time constant of the system. However, it is not feasible to meet this condition for stable reporter proteins and long cell doubling times where it is much more likely that $\tilde{T}_W \approx$ system dominant time constant.

One approach used successfully for an ensemble of *M* cell trajectories in an *E. coli* study assumed that the mean of the entire ensemble was zero, or

$$\frac{1}{M} \sum_{i=0}^{M} \frac{1}{\tilde{T}_W} \int_0^{\tilde{T}_W} \tilde{N}_m(t)dt = 0 \,,$$

which allowed the calculation of a single $D(t)$ that was applied to the correction of all cell trajectories[4]. This approach makes assumptions about very uniform local environmental conditions that may lead to significant errors if these assumptions are not valid. For example as illustrated below, this method applied to a population of cells displaying two different basal gene expression levels would lead to an ensemble of noise traces with a bimodal distribution and calculated autocorrelations that persist for erroneously long durations (Supplementary Fig. 2).

A second approach is to suppress the mean for each member of the ensemble (Supplementary Figure 2B), which requires finding $D_m(t)$ functions such that

$$\frac{1}{\widetilde{T}_W}\int_0^{\widetilde{T}_W}\widetilde{N}_m(t)dt = 0 .$$

The resulting ensemble of cell trajectories represent a zero mean stochastic process that is derived from, but is not equivalent to, the true gene expression stochastic process under study. The relationship between the true stochastic process ($F(t)$) and the one derived by removing the individual trajectory mean ($F_{SA}(t)$) is

$$F_{SA}(t) = F(t) - SA(t)$$

where $SA(t)$ is a piecewise continuous function given by

$$SA(t) = \frac{1}{\widetilde{T}_W}\int_0^{\widetilde{T}_W}F(t)dt \quad 0 \le t < \widetilde{T}_W$$
$$= \frac{1}{\widetilde{T}_W}\int_{\widetilde{T}_W}^{2\widetilde{T}_W}F(t)dt \quad \widetilde{T}_W < t < 2\widetilde{T}_W .$$

M

The autocorrelation function of $F_{SA}(t)$, $\Phi_{FSA}(\tau)$, is

$$\phi_{FSA}(\tau) = E[(F(t) - SA(t))(F(t+\tau) - SA(t+\tau))] =$$
$$E[F(t)F(t+\tau) + SA(t)SA(t+\tau) - F(t)SA(t+\tau) - F(t+\tau)SA(t)] =$$
$$\phi_F(\tau) + \phi_{SA}(\tau) - 2\phi_{F\cdot A}(\tau) ,$$

where the $E[\cdot]$ returns the expected value, $\Phi_F(\tau)$ is the autocorrelation of $F(t)$ (i.e. true autocorrelation), $\Phi_{SA}(\tau)$ is the autocorrelation of $SA(t)$, and $\Phi_{F\cdot A}(\tau)$ is the cross correlation between $SA(t)$ and $F(t)$.

Let us suppose that we can decompose $F(t)$ into two uncorrelated random processes ($F_c(t)$ and $F_u(t)$) such that

$$F(t) \approx F_c(t) + F_u(t)$$
$$\frac{1}{\widetilde{T}_W}\int_0^{\widetilde{T}_W} F_c(t)dt \to SA(t)$$
$$\frac{1}{\widetilde{T}_W}\int_0^{\widetilde{T}_W} F_u(t)dt \to 0$$

Then

$$\phi_{FSA}(\tau) = \phi_{F_u}(\tau) + \phi_{F_c}(\tau) + \phi_{SA}(\tau) - 2\left(\phi_{F_c \bullet A}(\tau) + \phi_{Fu \bullet SA}(\tau)\right)$$
$$\approx \phi_{F_u}(\tau) + \phi_{SA}(\tau) + \phi_{SA}(\tau) - 2\phi_{SA}(\tau) = \phi_{F_u}(\tau)$$

where the relationships

$$\phi_{F_c}(\tau) \approx \phi_{SA}(\tau)$$
$$\phi_{F_c \bullet A}(\tau) \approx \phi_{SA}(\tau)$$
$$\phi_{F_u \bullet A}(\tau) \approx 0$$

were used. The interpretation is that the autocorrelation function measured using this baseline suppression method is the autocorrelation of the fluctuations that lose correlation quickly compared to the duration of the single cell trajectories. We refer to the ACFs found using these baseline-suppressed individual trajectories as high frequency ACFs.

Mapping Between High Frequency and True Half Correlation Times

As described elsewhere and summarized in the main text, both positive and negative feedback shift the half correlation time, and this shift may be used to identify and quantify the

strength of feedback. Likewise, shifts in the half correlation time of the high frequency ACFs may be used to identify and quantify the strength of feedback if the mapping between true and high frequency half correlation times can be determined.

We performed a frequency domain analysis of the noise in the Tat circuit assuming that transcription was the dominant noise source[10]. That is, translational noise, extrinsic noise, and operator noise[11, 12] were assumed to be negligible. We assumed transcriptional noise to be a white noise source such that its power spectral density (PSD), $S_{tsc}(f)$, was constant ($S_{tsc}(f) = S_{tsc}(0)$). Accordingly, the PSDs of the noise in the Tat and GFP populations were found from [4, 9, 13]

$$S_{Tat}(f) = H^2_{tsc-Tat}(f) S_{tsc}(f) = H^2_{tsc-Tat}(f) S_{tsc}(0)$$
$$S_{GFP}(f) = H^2_{tsc-GFP}(f) S_{tsc}(f) = H^2_{tsc-GFP}(f) S_{tsc}(0)$$

where $H^2_{tsc-Tat}(f)$ and $H^2_{tsc-GFP}(f)$ are the noise power transfer functions [4, 9, 13,14] from the transcriptional noise source to Tat and GFP populations respectively, and were found using frequency domain analysis techniques described in[4, 9, 13] as

$$H^2_{tsc-Tat}(f) \approx K_{Tat} \frac{1}{\left(1+\left(\frac{f}{(1-T)f_{Tat}}\right)^2\right)\left(1+\left(\frac{f}{f_{mRNA}}\right)^2\right)\left(1+\left(\frac{f}{f_{OP}}\right)^2\right)}$$

$$H^2_{tsc-GFP}(f) \approx K_{GFP} \frac{\left(1+\left(\frac{f}{f_{Tat}}\right)^2\right)}{\left(1+\left(\frac{f}{f_{GFP}}\right)^2\right)\left(1+\left(\frac{f}{(1-T)f_{Tat}}\right)^2\right)\left(1+\left(\frac{f}{f_{mRNA}}\right)^2\right)\left(1+\left(\frac{f}{f_{OP}}\right)^2\right)},$$

where K_{Tat} and K_{GFP} have no frequency dependence, f_{OP} represents all other rate limiting processes (e.g. protein folding and maturation) not captured in mRNA and protein decay and dilution, and the feedback strength (T) is

$$T = \frac{\beta k_{p-Tat} k_m}{\gamma_{mRNA}\gamma_{Tat}}.$$

We used the following definition for the preceding analysis:

f = frequency in Hz

$f_{mRNA}, f_{GFP}, f_{Tat}$ are frequencies associated with mRNA, GFP, and Tat decay and dilution = $\gamma/2\pi$ where γ is the decay/dilution rate constant for the molecular species

γ_{mRNA}, γ_{GFP}, γ_{Tat} are the decay/dilution rate constants for mRNA, GFP, and Tat

k_m is the transcription rate constant

$k_{p\text{-}Tat}$ and $k_{p\text{-}GFP}$ are the translation rate constants for Tat and GFP respectively

k_p is the translation rate constant

β is a factor representing the Tat-modulation of transcription rate. Here we assume no frequency limitations for this modulation

The measured signal comes from the GFP, and frequency independent terms (K_{GFP} and $S_{tsc}(0)$) have no effect on the normalized autocorrelation functions. Consequently, we only need to consider the normalized $S_{GFP}(f)$:

$$S_{GFP}(f) \approx \frac{\left(1+\left(\frac{f}{f_{Tat}}\right)^2\right)}{\left(1+\left(\frac{f}{f_{GFP}}\right)^2\right)\left(1+\left(\frac{f}{(1-T)f_{Tat}}\right)^2\right)\left(1+\left(\frac{f}{f_{mRNA}}\right)^2\right)\left(1+\left(\frac{f}{f_{OP}}\right)^2\right)}$$

The GFP PSD is more complex than the Tat PSD as it has a zero and an extra pole, and note that the zero and extra pole cancel if either T=0 (i.e. no feedback) or if GFP and Tat decay/dilution rates are equal.

For low values of T the ordering (from lowest to highest) of the frequencies associated with the poles and zero is: f_{GFP} (due to long decay time of GFP), $(1\text{-}T)f_{Tat}$, f_{Tat}, and f_{mRNA}/f_{OP}. Increasing values of T push the $(1\text{-}T)f_{Tat}$ pole lower in frequency but do not alter the ordering of the poles and zero until $T > 1 - f_{GFP}/f_{Tat}$. For larger values of T the ordering of the poles becomes: $(1\text{-}T)f_{Tat}$, f_{GFP}, and f_{mRNA}/f_{OP}. Thus as a function T there are two GFP PSD regimes:

1. $0 \le T \le 1 - f_{GFP}/f_{Tat}$: increasing values of T move the second pole and the zero further apart (they are equal for T=0) with the result that higher frequency noise is reduced relative to the low frequency noise.
2. $1 - f_{GFP}/f_{Tat} \le T \le 1$: frequencies of the zero and second pole remain fixed at f_{Tat} and f_{GFP}, while increasing values of T move the first pole, $(1\text{-}T)f_{Tat}$, to lower frequencies.

To calculate the mapping between the high frequency and real half correlation times we constructed a simplified model of the GFP PSD given by

$$S_{GFP}(f) \approx \frac{1}{\left(1+\left(\frac{f}{f_{GFP}}\right)^2\right)\left(1+\left(\frac{f}{f_{eff}(T)}\right)^2\right)}$$

where f_{eff} is a T-dependent pole that approximates the effects of the attenuation of high frequency noise by the zero-2nd pole combination and the higher frequency poles. We approximated the T-dependence of f_{eff} and accounted for the two regimes listed above as follows:

$$f_{eff} = f_{eff\_u} - \left(\frac{T}{1 - f_{GFP}/f_{Tat}}\right)\left(f_{eff\_u} - f_{eff\_l}\right) \qquad 0 \le T \le 1 - f_{GFP}/f_{Tat}$$
$$f_{eff} \approx f_{eff\_l} \qquad 1 - f_{GFP}/f_{Tat} < T \le 1$$

,

where f_{eff_u} and f_{eff_l} are the upper and lower boundaries of possible f_{eff} values.

Construction of the high frequency $\tau_{1/2} - T$ calibration curve was performed through the exact stochastic simulation of the simple model using various values of T (see error estimation section below). The output of the simulations was divided into 12 hour segments and processed exactly as the data from the measurements. The parameter values were found using the following two steps to fit the curve to the two extremes of T:

1. Determining values of f_{GFP} and f_{eff_u} from the T=0 (control circuit) measurements. These selections were made to be consistent with long GFP half life, relatively long cell doubling times, and reasonable assumptions about mRNA half life.
2. Determining values of f_{Tat} and f_{eff_l} with the assumption that T --> 1 for the circuits with the largest positive feedback (e.g. LTR-GFP-Tat). These selections were made to be consistent with published values of Tat half life.

The three different T=0 conditions (no drug, +Tat, and + TNFα) resulted in different values of $\tau_{1/2}$ (1.2 hours, 1.37 hours, and 1.29 hours, respectively). These variations were larger than the error bars and likely indicate that the different induction mechanisms have moderately different basal noise characteristics. To account for these different basal noise characteristics, measured $\tau_{1/2}$ values were normalized to the $\tau_{1/2}$ value for the corresponding no feedback circuit. That is,

$\tau_{1/2}$ for LTR-GFP-Tat no drug was normalized to $\tau_{1/2}$ for LTR-GFP no drug; $\tau_{1/2}$ for LTR-GFP-Tat +Tat was normalized to $\tau_{1/2}$ for LTR-GFP +Tat; $\tau_{1/2}$ for LTR-GFP-Tat + TNFα was normalized to $\tau_{1/2}$ for LTR-GFP + TNFα.

Supplementary Figure 3 shows a calibration curve constructed as described above. There is a clear break between the two regimes that is an artifact of the relative simplicity of the model. The actual relationship would likely resemble the smoother curve shown in the figure. However, the behavior in the two regimes (strong *T* dependence for lower values of *T*, weak *T* dependence for higher values) is well captured by the piecewise linear approximation. Errors in the calibration curve are mostly associated with assumptions made in the two-step parameter estimation described above. In particular, the break point between the two regimes is determined by the ratio of GFP and Tat decay/dilution rates, so the "real" transition between these regimes will depend on the "real" ratio of these rates. However, large variations from the ratio we used would not be consistent with the high frequency $\tau_{1/2}$ values we measured.

Perhaps the major advantage to this method is that a relatively short duration measurement (i.e. 12 hours) provides insight about much longer term (i.e. 30-72 hour) dynamics. That is, the extension of the transient pulse unfolds over a time period of days, but the magnitude of this extension is determined by the strength of the positive feedback, which can be estimated from the 12 hour measurements. Furthermore, this method is much more sensitive to correlation shifts caused by feedback than those caused by some other possible mechanisms. Most notably, the high frequency $\tau_{1/2}$ has a very weak dependence on changes in the dominant time constant (that is why the calibration curve is so flat for the high T values). Thus, if correlation shifts in the real $\tau_{1/2}$ were due to changes in GFP half life or dilution rate (i.e. cell growth rate), these shifts would be weakly reflected in the high frequency $\tau_{1/2}$. However, the associated limitation is that

while this method easily differentiates between low and high feedback strengths, it provides a relatively poor ability to differentiate between two different high values of *T*.

Half-Correlation Time Error Bar Estimation

We estimated the error bars on the high frequency $\tau_{1/2}$ measurements using exact stochastic simulation of the simplified 2-pole model described above. Stochastic simulation software (BioSpreadsheet; available for download at http://biocomp.ece.utk.edu) was used to generate time series data, and custom software was used to generate composite autocorrelation functions using a selected number (M) of single cell trajectories. From the simulations several different collections of cells were created for each value of M and the high frequency $\tau_{1/2}$ for each of these collections was calculated. The collections of cells were selected from a simulated population of 3000 uncorrelated 12 hour single cell trajectories. The standard deviation in the high frequency $\tau_{1/2}$ was calculated for each value of M. All stochastic simulations were based on variations of the Gillespie stochastic simulation algorithm[15-17].

The stochastic 2-pole model simulated was as follows:

Reaction	Rate
1. $G \rightarrow G + M$	k_M
2. $M \rightarrow M + P$	k_P
3. $M \rightarrow *$	γ_M
4. $P \rightarrow *$	γ_p

The lowest frequency pole (f_{GFP} or $(1-T)f_{Tat}$ depending upon the value of T) was set by reaction 4 to be $\gamma_p/2\pi$. The second pole (f_{eff}) was set by reaction 3 to be to be $\gamma_m/2\pi$. To simulate different values of T for the calibration curve (Supplementary Fig. 3) the half life of species P was set to 7 hours in the first regime and $(4.375/(1-T))$ in the 2nd regime, while the half life of species M, $t_{1/2\text{-}M}$, was set as follows:

$$t_{1/2-M} = 10 + \left(\frac{T}{1 - f_{GFP}/f_{Tat}}\right)(60-10)\text{min} \qquad 0 \le T \le 1 - f_{GFP}/f_{Tat}$$
$$t_{1/2-M} = 10\,\text{min} \qquad 1 - f_{GFP}/f_{Tat} < T \le 1$$

Finally, M and P production rates were set by using a burst of 100 and $\langle M \rangle = 10$ for all simulated experiments and T ranges.

Pitfalls of Fluorescence Magnitude as a Measure of Positive Autoregulation Strength

Positive autoregulation strength may also be inferred from a comparison of the magnitude of GFP fluorescence in circuits with and without feedback. However, there are potential pitfalls to this method that should be considered. Firstly, positive feedback (+FB) mediated increases in GFP expression may be difficult to differentiate from other mechanisms that increase measured fluorescence, which include (i) differing levels of basal expression from the promoter (perhaps due to different chromosomal integration sites), (ii) different local concentrations of inducers, and (iii) instrumental effects of different gains in fluorescence detection. Furthermore, timing issues can confound magnitude analysis, since circuits with +FB may take significantly more time to reach their full induction level than non-feedback circuits.

To illustrate these issues we consider two cases analytically: (1) gene expression from circuits that have not been induced (the equilibrium case); and (2) gene expression from circuits that experience a step increase in expression due to the addition of a chemical inducer (the non-equilibrium case). In each case the subscript FB will indicate a circuit that has +FB while the subscript NFB indicates the absence of autoregulation. For case (1) we may write

$$\frac{d[Tat]_{NFB}}{dt} = \alpha_{NFB} - \gamma[Tat]_{NFB}$$

$$[Tat]^{SS}_{NFB} = \frac{\alpha_{NFB}}{\gamma}$$

$$\frac{d[Tat]_{FB}}{dt} = \alpha_{FB} + k[Tat]_{FB} - \gamma[Tat]_{FB}$$

$$[Tat]^{SS}_{FB} = \frac{\alpha_{FB}}{\gamma - k}$$

where $[Tat]^{SS}$ is the steady-state level of Tat, α is the basal level of expression, γ is the protein decay/dilution rate, and k is the rate of Tat self-induction. Then, feedback-strength is

$\frac{[Tat]^{SS}_{FB}}{[Tat]^{SS}_{NFB}} = \frac{\alpha_{FB}\gamma}{(\gamma - k)\alpha_{NFB}}$ which reduces to $\frac{[Tat]^{SS}_{FB}}{[Tat]^{SS}_{NFB}} = \frac{\gamma}{(\gamma - k)} = \frac{1}{1 - T}$

if, and only if, the basal expression levels are equal (i.e. $\alpha_{FB} = \alpha_{NFB}$).

However, different chromosomal integration sites often lead to significantly different basal expression levels for the LTR promoter (an order of magnitude or more variation has been observed) which can greatly compromise the accuracy of the measured feedback strength. Thus, even for the equilibrium case, fluorescence magnitude can only be reliably used as a measure of feedback-strength when different clones are known to have approximately equivalent basal expression levels.

For case (2), where the circuit has experienced a step increase in expression, we may write

$$\frac{d[Tat]_{NFB}}{dt} = \alpha_{NFB} + \alpha_I U(t) - \gamma[Tat]_{NFB}$$

$$[Tat]^{SS}_{NFB} = \frac{\alpha_{NFB}}{\gamma} + \frac{\alpha_I}{\gamma}\left(1 - e^{-\gamma t}\right)$$

$$\frac{d[Tat]_{FB}}{dt} = \alpha_{FB} + \alpha_I U(t) + k[Tat]_{FB} - \gamma[Tat]_{FB},$$

$$[Tat]^{SS}_{FB} = \frac{\alpha_{FB}}{\gamma - k} + \frac{\alpha_I}{\gamma - k}\left(1 - e^{-(\gamma - k)t}\right)$$

$$\textbf{\textit{Then :}}\ \frac{[Tat]^{SS}_{FB}}{[Tat]^{SS}_{NFB}} = \frac{\frac{\alpha_{NFB}}{\gamma} + \frac{\alpha_I}{\gamma}\left(1 - e^{-\gamma t}\right)}{\frac{\alpha_{FB}}{\gamma - k} + \frac{\alpha_I}{\gamma - k}\left(1 - e^{-(\gamma - k)t}\right)}$$

where $U(t)$ is a unit step function and we have assumed that gene expression has not saturated for either of the two circuits (if the +FB circuit does reach saturation, the FB/NFB ratio has little quantitative meaning). If, and only if, the step increase in expression is large compared to basal expression for both circuits, the ratio reduces to

$$\frac{[Tat]^{SS}_{FB}}{[Tat]^{SS}_{NFB}} = \frac{(\gamma - k)\left(1 - e^{-\gamma t}\right)}{\gamma\left(1 - e^{-(\gamma - k)t}\right)} \approx \frac{1}{1 - T} \Leftrightarrow t >> \frac{1}{\gamma - k}.$$

Conversely, if the NFB circuit basal expression is not negligible compared to its induced level, the fluorescence level is a poor quantitative measure of feedback strength. Furthermore, the circuit with +FB may take quite some time to reach full induction (e.g. > 60 hours for T > 0.8). To accurately measure +FB strength, the concentration of inducer and other environmental conditions that control gene expression must remain constant for this entire period, which may be a difficult constraint to meet.

Constructs and clones

The LTR-GFP and LTR-GFP-Tat constructs are lentiviral vectors whose cloning we have previously described [1]. Briefly, the LTR-GFP-Tat positive-feedback construct described in this

study encodes an Internal Ribosomal Entry Sequence (IRES) between GFP and Tat in order to allow bi-cistronic and stoichoimetrically linked expression of GFP and Tat from a single mRNA. These lentiviral constructs were used to create stable isogenic Jurkat T-cell lines containing single-integrations as previously described[1]. The J-lat clonal cell line (J-Lat Full Length Clone 10.6) was obtained through the NIH AIDS Research and Reference Reagent Program, Division of AIDS, NIAID, NIH from Dr. Eric Verdin[2].

Single-cell time-lapse microscopy and flow cytometry

Jurkat T-cells were imaged on a Perkin-Elmer UltraView Spinning Disk Confocal microscope fitted with a live-cell chamber (Bioptechs, Butler, PA). All experiments were performed at 37°C under CO_2 using a 10X-dry or heated 20X-immersion objective. Cells were immobilized by incubation in glass-bottom cell-culture dishes (Matek Corp., Ashland, MA) for 1 h, drug perturbations were applied, and images were captured every 5-10 minutes for 12-15 h at an acquisition speed of 100-1000 msec depending on the experiment. Images and movies were acquired using the Perkin-Elmer UltraView™ software and custom Matlab™ (Mathworks) code was used to perform single-cell segmentation and tracking (see representative 6 hour 40 minute duration movie of single cell tracking provided along with the supplementary material). We have previously described this technique [3, 4].

Flow cytometry and FACS sorting parameters are as follows: living cells (in growth media) were gated on forward- vs. side- scattering and sorted according to the level of GFP expression. At least 10,000 GFP events were recorded for each experiment and data was analyzed using FlowJo™ (Treestar Inc., Ashland Oregon).

Cell-culture and drug perturbations

Jurkat T-cells were maintained at densities between $2x10^5$-$2x10^6$ cells/ml at 37° C under CO_2 and humidity in RPMI 1640 supplemented with 10% fetal calf serum. The LTR-GFP-Tat Jurkat clone E7 and LTR-GFP Jurkat clones D5 and E11 were used throughout this study. These clones have been previously characterized [1]. TNF-α was obtained from Sigma Chemical Co. (St. Louis, MO), dissolved in DMSO, and used at final concentration of 10ng/ml while purified HIV-1 Tat protein was obtained from ABL Inc. (Kensington, MD) and cells were exposed to these perturbations as previously described [5]. Cell death was assayed by forward-scatter vs. side-scatter (and propidium-iodide uptake) flow cytometry analysis and TNF-α did not appear to be significantly cytotoxic to Jurkat cells over 48hrs as is shown below for LTR-GFP cells after TNF-α exposure (Supplementary Figure 4).

Quantitative Western analysis

Quantitative Western Blot analysis for Tat and GFP was performed as previously described[6]. Briefly, Jurkat cells were activated with TNFα for 4hrs (as per Hoffman et al. *Science* 2002*)*[7] washed 2x in PBS, and an aliquot of $6x10^6$ cells removed and frozen-down at the indicated time points. Lowry assay was used to load equivalent amounts of protein to each well on a 14% gel and an anti-FLAG antibody was used to quantify Tat (LTR-GFP-Tat contains a 2x FLAG tag on the 3' terminus of Tat) after transfer to a membrane, blocking, washing, and staining with ECL Plus™ reagent, blots were quantified on a Molecular Dynamics Typhoon™ imager. Band intensities were normalized relative to the α-Tubulin control (antibody: Santa Cruz #5286; anti-mouse, used at 1:5000) and to the 4hr TNF time-point (Supplementary Figure 5). We are grateful

to Shannon Werner and the Hoffman Signaling Systems Lab, UCSD, for technical assistance and advise.

References

1. Weinberger, L. S., Burnett, J. C., Toettcher, J. E., Arkin, A. P. & Schaffer, D. V. Stochastic gene expression in a lentiviral positive-feedback loop: HIV-1 Tat fluctuations drive phenotypic diversity. Cell 122, 169-82 (2005).
2. Jordan, A., Bisgrove, D. & Verdin, E. HIV reproducibly establishes a latent infection after acute infection of T cells in vitro. Embo J 22, 1868-77 (2003).
3. Weinberger, L. S. & Shenk, T. An HIV Feedback Resistor: Auto-Regulatory Circuit Deactivator and Noise Buffer. PLoS Biol 5, e9 (2006).
4. Austin, D. W. et al. Gene network shaping of inherent noise spectra. Nature 439, 608-11 (2006).
5. Jordan, A., Defechereux, P. & Verdin, E. The site of HIV-1 integration in the human genome determines basal transcriptional activity and response to Tat transactivation. Embo J 20, 1726-38 (2001).
6. Weinberger, L. S. & Shenk, T. An HIV feedback resistor: auto-regulatory circuit deactivator and noise buffer. PLoS Biol 5, e9 (2007).
7. Hoffmann, A., Levchenko, A., Scott, M. L. & Baltimore, D. The IkappaB-NF-kappaB signaling module: temporal control and selective gene activation. Science 298, 1241-5 (2002).
8. Bendat, J. S. & Piersol, A. G. Data: Analysis and Measurement Procedures (Wiley, New York, 2000).
9. Cox, C. D. et al. Frequency domain analysis of noise in simple gene circuits. Chaos 16, 026102 (2006).
10. Thattai, M. & van Oudenaarden, A. Intrinsic noise in gene regulatory networks. Proceedings of the National Academy of Sciences of the United States of America 98, 8614-8619 (2001).
11. Kepler, T. B. & Elston, T. C. Stochasticity in transcriptional regulation: Origins, consequences, and mathematical representations. Biophysical Journal 81, 3116-3136 (2001).
12. Simpson, M. L., Cox, C. D. & Sayler, G. S. Frequency domain chemical Langevin analysis of stochasticity in gene transcriptional regulation. Journal of Theoretical Biology 229, 383-394 (2004).
13. Simpson, M. L., Cox, C. D. & Sayler, G. S. Frequency domain analysis of noise in autoregulated gene circuits. Proc Natl Acad Sci U S A 100, 4551-6 (2003).
14. Supplementary Information of Austin et al., Nature 439, Feb. 2, 2006.
15. Gillespie, D. T. Exact Stochastic Simulation of Coupled Chemical-Reactions. Journal of Physical Chemistry 81, 2340-2361 (1977).
16. Gillespie, D. T. General Method for Numerically Simulating Stochastic Time Evolution of Coupled Chemical-Reactions. Journal of Computational Physics 22, 403-434 (1976).
17. Gibson, M. A. & Bruck, J. Efficient exact stochastic simulation of chemical systems with many species and many channels. Journal of Physical Chemistry A 104, 1876-1889 (2000).

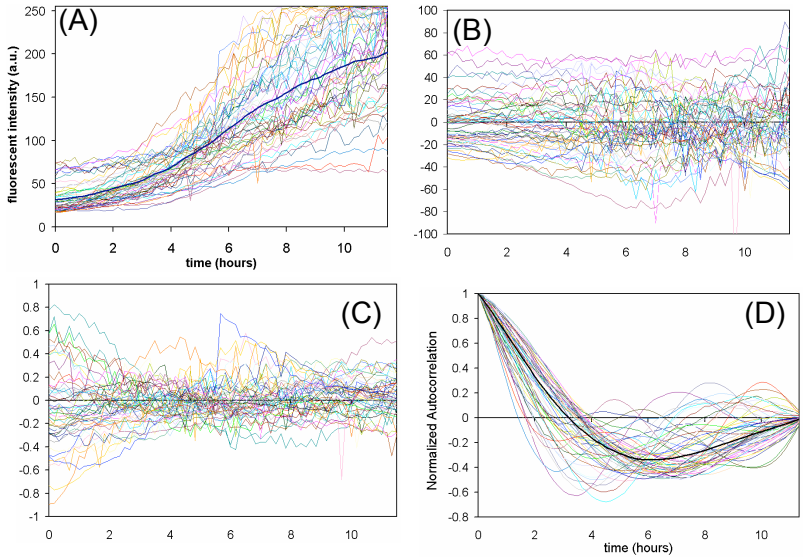

Supplementary Figure 1: (A) Measured fluorescence intensities ($I_m(kT_s)$), the general trend ($A(kT_s)$; dark solid line), and (B) after removal of the general trend ($I_m(kT_s)$-$g_mA(kT_s)$). (C) Scaling and baseline removal to obtain $\widetilde{N}_m(t)$. (D) The normalized autocorrelation functions for the individual trajectories (in color) and the normalized composite autocorrelation function (black curve).

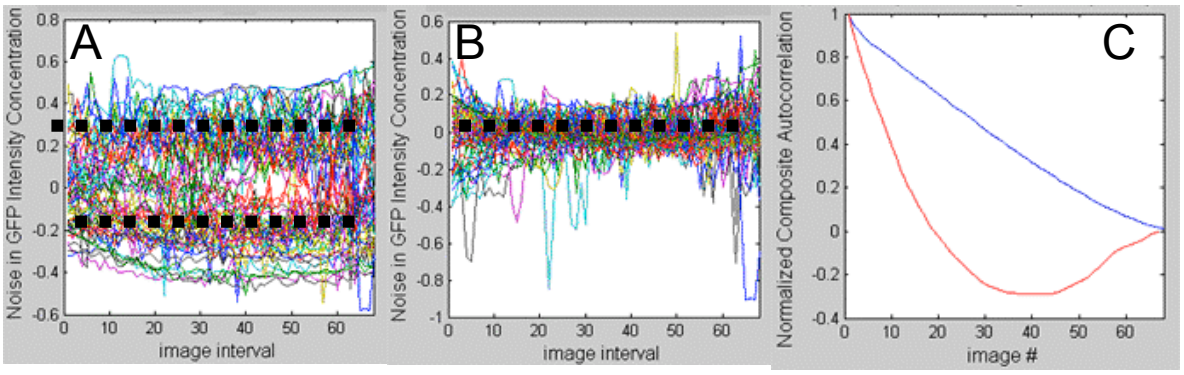

Supplementary Figure 2: (A) Noise trajectories after general trend removal and the application of a baseline correction that satisfies the relationship $\frac{1}{M}\sum_{i=0}^{M}\frac{1}{\tilde{T}_W}\int_0^{\tilde{T}_W}\tilde{N}_m(t)dt = 0$. The signals are distributed around two different baselines (dashed dark lines) indicative of a colony with two different basal expression levels. (B) The same group of traces as in (A) but the baseline correction has been made to satisfy the relationship $\frac{1}{\tilde{T}_W}\int_0^{\tilde{T}_W}\tilde{N}_m(t)dt = 0$. (C) The normalized composite autocorrelation functions for the signals in (A; blue) and in (B; red). The blue autocorrelation is saturated (i.e. has a linear decay that is entirely due to the biasing algorithm) and is not related to the underlying stochastic process. In contrast, the red autocorrelation function has a decay that is largely driven by the higher frequency fluctuations in the signals in (B) as described below.

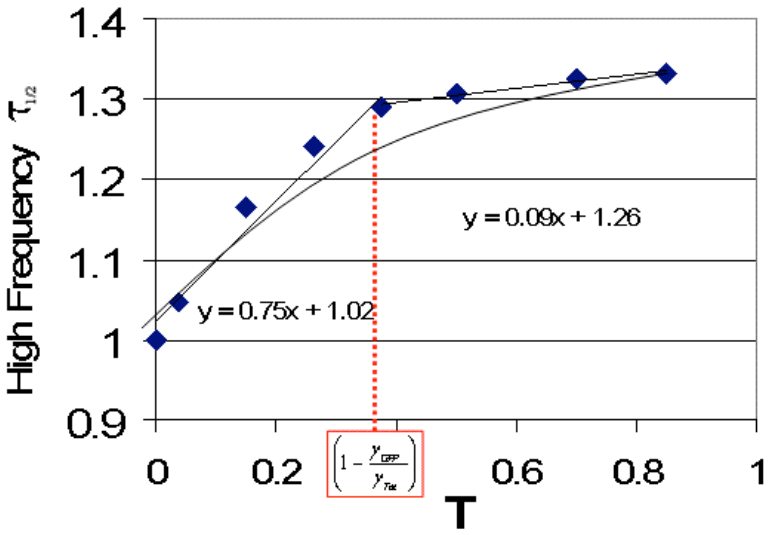

Supplementary Figure 3: Calibration curve relating the values of T and the high frequency $\tau_{1/2}$. The high frequency $\tau_{1/2}$ values are normalized to the T=0 (no feedback) $\tau_{1/2}$ value.

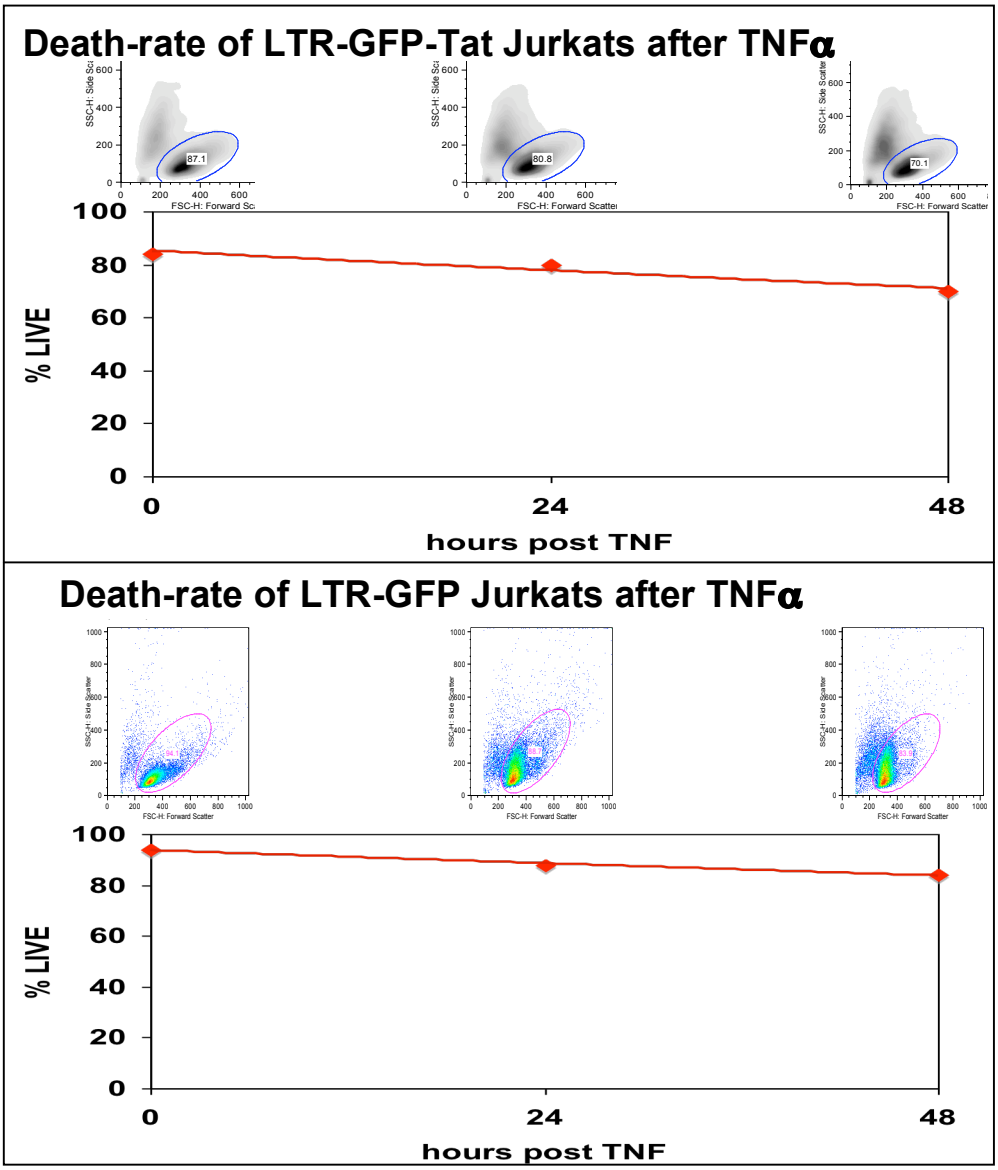

Supplementary Figure 4: TNF-α is not significantly cytotoxic to Jurkat cells over 48hrs. Upper Panel: Forward-scatter vs. Side-scatter flow cytometry of LTR-GFP-Tat cells after TNF-α exposure (percentage in live gate is plotted in graph). Lower panel: Forward-scatter vs. side-scatter flow cytometry of LTR-GFP cells after TNF-α exposure (percentage in live gate is plotted in graph).

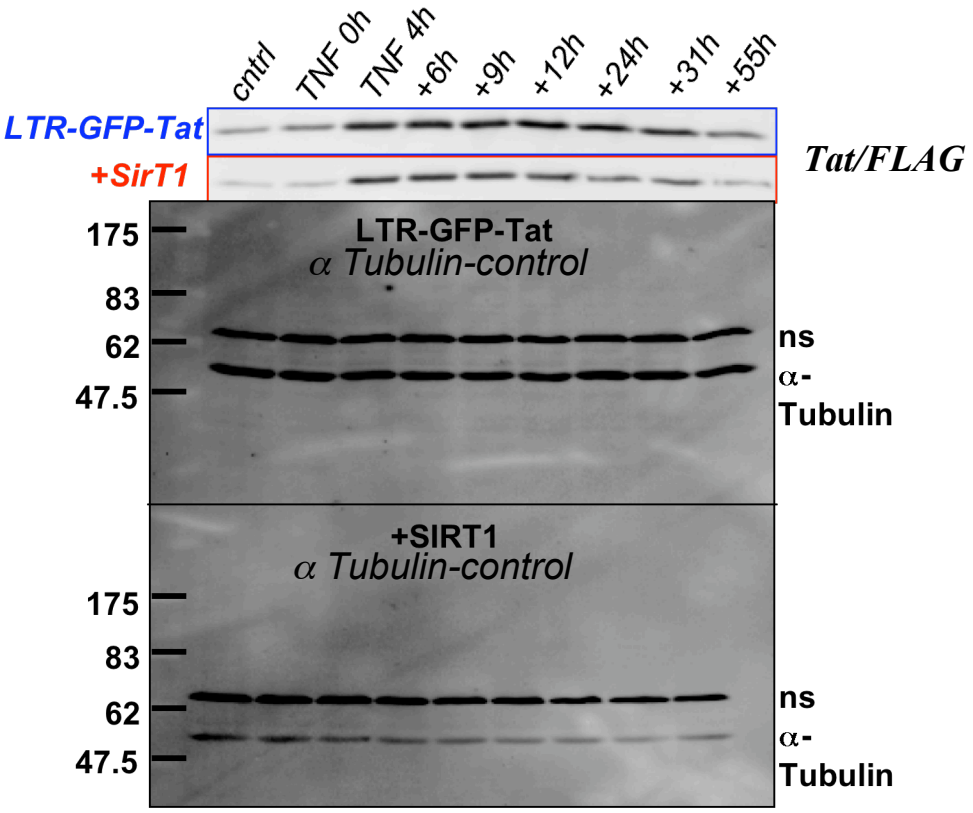

Supplementary Figure 5: Quantitative Western Blot analysis for Tat(2xFLAG) and GFP in LTR-GFP-Tat and LTR-GFP-Tat +SirT1 cells after 4hr TNF activation pulse. Tat and Tubulin blots were run/stained in parallel and developed on the same film. Tat band (upper) ran at ~11kDa. α-Tubulin control band is at 55kD (α-Tubulin control antibody shows a non-specific upper band at around 65kD). We are grateful to Shannon Werner and the Hoffman Signaling Systems Lab, UCSD, for technical assistance and advise.

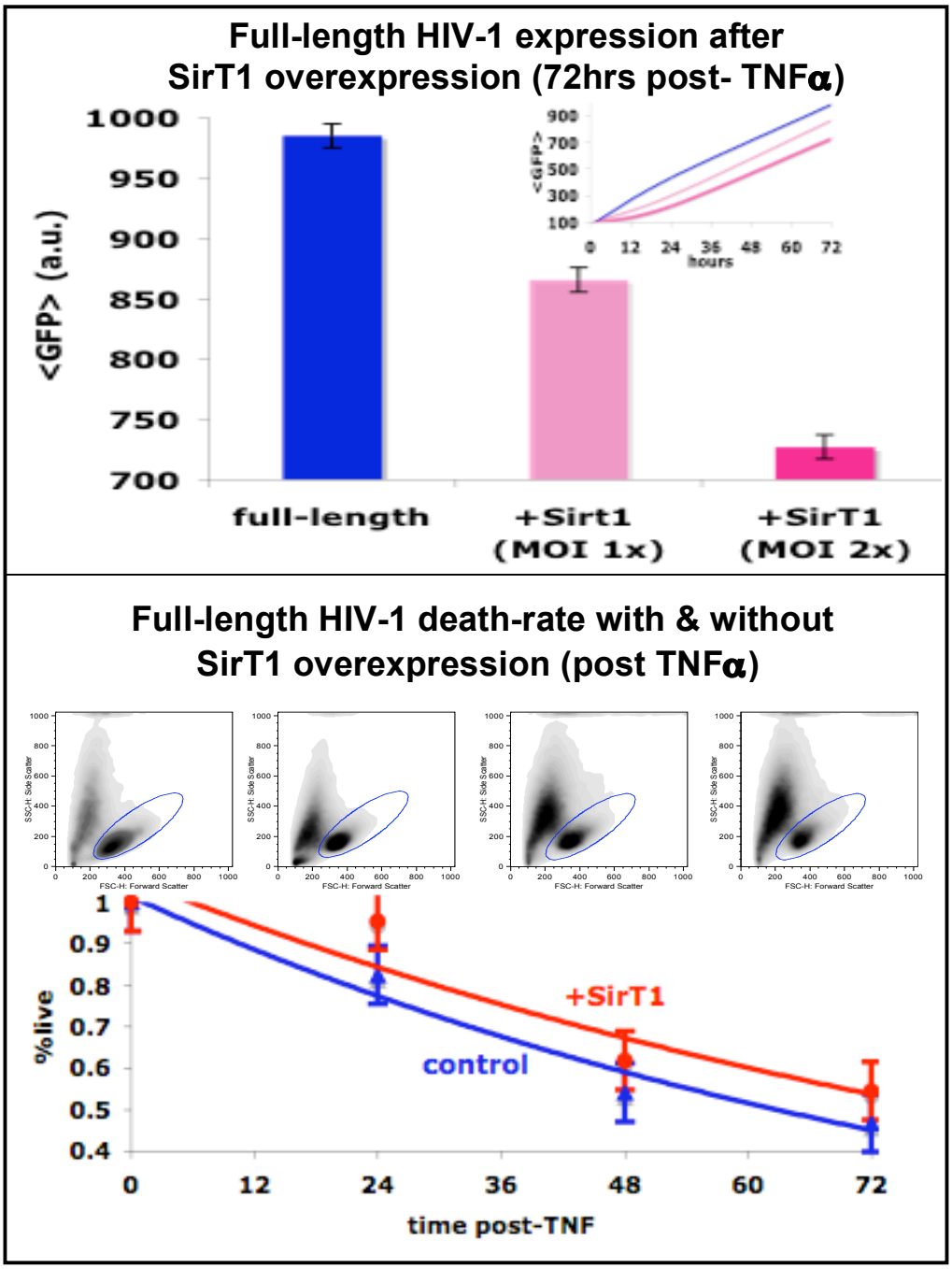

<u>Supplementary Figure 6</u>: **Increasing SirT1 over-expression decreases full-length HIV-1 transactivation but does not eliminate lytic gene expression**: Upper Panel: Increasing SirT1 retrovirus multiplicity of infection (MOI) decreases full-length HIV-1 transactivation levels in single-cells in a titrated fashion; data collected 72hrs post TNF-α activation, inset shows single-cell flow cytometry trajectories 0hrs-72hrs. Lower panel: Death rates for full-length HIV-1 (J-lat) cells over-expressing SirT1.

Supplementary Table 1: Summary Table of Reported Experimental Composite $\tau_{1/2}$ and Strength of Regulation (T) Values (error estimation discussion at the end).

	Experiment	$\tau_{1/2}/\tau_{1/2\text{-NFB}}$	# of cells accounted for	Estimated T [See Note below]
1.	LTR-GFP No Drug	1	31	0
2.	LTR-GFP + Tat	1	43	0
3.	LTR-GFP + TNFα	1	30	0
4.	LTR-GFP-Tat No Drug	1.33 (±0.06)	77	0.9 (+0.1, -0.4)
5.	LTR-GFP-Tat + Tat	1.29 (±0.06)	71	0.6 (±0.4)
6.	LTR-GFP-Tat + TNFα	1.29 (±0.07)	57	0.6 (±0.4)
7.	LTR-GFP-Tat – SirT1 overexpressed + TNFα	1.19 (±0.05)	94	0.22 (±0.07)
8.	LTR-GFP-Tat k50A mutant + TNFα	1.2 (±0.06)	63	0.23 (±0.08)
9.	Full length HIV-1 + TNFα	1.38 (±0.09)	41	0.97 (+0.03, -0.37)

Note: Measurements made with no added inducer (No Drug) were uniformly found to have a lower $\tau_{1/2}$ than those with added TNFα, which were lower than those with added Tat. These measurements suggest an inducer-mediated shift in noise correlation that is accounted for in the calibration curve by normalizing each measurement to the corresponding no feedback measurement.